Dissecting the Domain Structure of Cdc4p, a Myosin Essential Light Chain Involved in Schizosaccharomyces pombe Cytokinesis †

ARTICLE *in* BIOCHEMISTRY · OCTOBER 2005

Impact Factor: 3.02 · DOI: 10.1021/bi050641c · Source: PubMed

Dissecting the Domain Structure of Cdc4p, a Myosin Essential Light Chain Involved in *Schizosaccharomyces pombe* Cytokinesis†

Eric Escobar-Cabrera,‡ Meenakshi Venkatesan,‡ Michel Desautels,§ Sean M. Hemmingsen,§ and Lawrence P. McIntosh*,‡

Department of Biochemistry and Molecular Biology, Department of Chemistry, The Michael Smith Laboratories, and The Protein Engineering Network of Centres of Excellence, University of British Columbia, Vancouver, British Columbia, Canada V6T 1Z3, Department of Microbiology and Immunology, University of Saskatchewan, Saskatoon, Saskatchewan, Canada S7N 5E5, and The Plant Biotechnology Institute, National Research Council of Canada, 110 Gymnasium Place, Saskatoon, Saskatchewan, Canada S7N 0W9

Received April 6, 2005; Revised Manuscript Received July 14, 2005

ABSTRACT: Cytokinesis is the process by which one cell divides into two. Key in the cytokinetic mechanism of *Schizosaccharomyces pombe* is the contractile ring myosin, which consists of two heavy chains (Myo2p), two essential light chains (Cdc4p), and two regulatory light chains (Rlc1p). Cdc4p is a dumbbell-shaped EF-hand protein composed of N- and C-terminal domains separated by a flexible linker. The properties of these two domains are of particular interest because each is hypothesized to have independent functions in binding different components of the cytokinesis machinery. To help define these properties, we used NMR spectroscopy to compare the structure, stability, and dynamics of the isolated N- and C-terminal domains with one another and with native Cdc4p. On the basis of invariant chemical shifts, the N-domain retains the same structure in isolation as in the context of the full-length Cdc4p, whereas the C-domain appears markedly perturbed. This perturbation results from intramolecular binding of the residual linker sequence at the N-terminus of the C-domain in a mode similar to that used by native Cdc4p to associate with target polypeptide sequences. NMR relaxation, thermal denaturation, and amide hydrogen exchange experiments also indicate that the C-domain is less stable and more dynamic than the N-domain, both in isolation and in the full-length protein. We hypothesize that these properties reflect a conformational plasticity of the C-domain, which may allow Cdc4p to interact with several regulatory or contractile ring proteins necessary for cytokinesis.

Research on cell division has been ongoing since the 19th century, and although significant progress has been achieved, it is still unclear how this process works precisely at the molecular level (*1*). Understanding the mechanisms and the regulation of cell division is of great importance not only because of the fascinating coordination of the cytoskeletal "nanomachinery" but also because proteins involved in cell division are targets for drug design to treat diseases such as cancer (*2*).

The final stage of cell division is known as cytokinesis. In most organisms, the cell divides into two via the contraction of an actin−myosin ring (*3*). The contractile ring responsible for cytokinesis contains, among other proteins, actin and myosin, a well-characterized molecular motor. Type II myosin is a hexamer composed of two heavy chains, two essential light chains (ELC),[1] and two regulatory light chains (RLC) (*4*). One of the model organisms for characterizing cytokinesis at the molecular level is the fission yeast *Schizosaccharomyces pombe* (*5*). In *S. pombe*, there are two type II myosins. Myo2p is the main myosin heavy chain of the contractile ring, while Myp2p is nonessential and required by cells under conditions of stress (*6*). Co-immunoprecipitation and genetic studies have shown that the essential and regulatory light chains are Cdc4p (*7*, *8*) and Rlc1p (*9*, *10*), respectively. Myo2p has two IQ motifs (IQxxxRGxxxR, where "x" is any residue), with Cdc4p binding principally to IQ1 and Rlc1p to IQ2 (*8*, *9*, *11*).

Similar to calmodulin (*12*−*16*), troponin C (*17*−*20*), and the myosin light chains (*21*, *22*), Cdc4p is a dumbbell-shaped protein composed of N- and C-terminal EF-hand domains

† Supported by grants from the National Cancer Institute of Canada with funds from the Canadian Cancer Society (to L.P.M.) and by the St. John's College Charles C. C. Wong Memorial and Sir Quo-Wei Lee Fellowships (to E.E.-C.). Instrument support was provided by the Government of Canada's Network of Centres of Excellence Program supported by the Canadian Institutes of Health Research (CIHR) and the Natural Sciences and Engineering Research Council (NSERC) through the Protein Engineering Network of Centres of Excellence (PENCE, Inc.). L.P.M. is a CIHR Scientist.

* To whom correspondence should be addressed. Phone: 604-822-3341. Fax: 604-822-5227. E-mail: mcintosh@chem.ubc.ca.

‡ University of British Columbia.

§ University of Saskatchewan and National Research Council of Canada.

[1] Abbreviations: ATCUN, amino-terminal Cu^{2+} (Ni^{2+}) binding; Cdc4p-C, residues 72−141 of Cdc4p plus an N-terminal Gly-Ser-His; Cdc4p-Cs, residues 76−141 of Cdc4p; Cdc4p-N, residues 1−75 of Cdc4p plus an N-terminal Gly-Ser-His; ELC, essential light chain; HSQC, heteronuclear single-quantum correlation; HX, hydrogen exchange; MWCO, molecular weight cutoff; pH*, observed pH meter reading without correction for isotope effects; RLC, regulatory light chain; rms, root mean squared; T_m, midpoint thermal unfolding temperature.

10.1021/bi050641c CCC: $30.25
Published on Web 08/19/2005

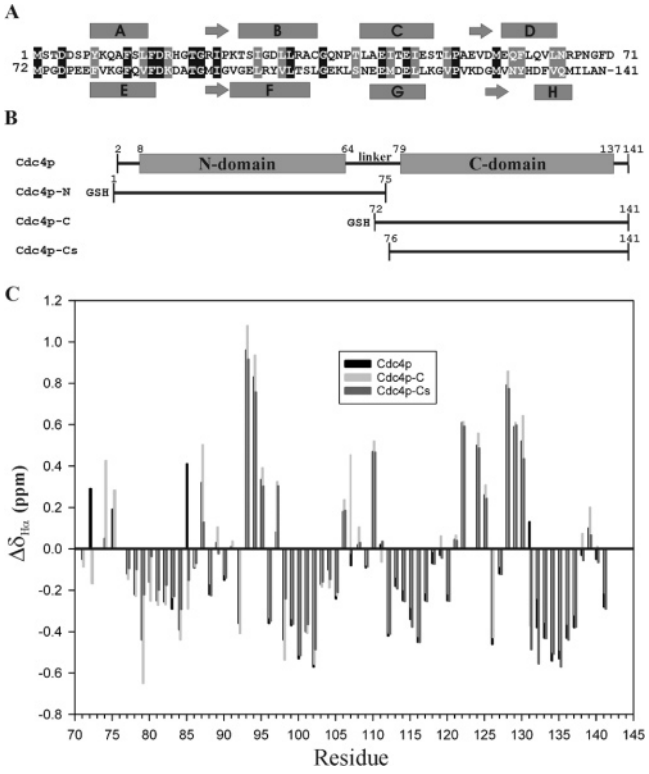

FIGURE 1: (A) Sequence alignment of the N- and C-domains of Cdc4p. α-Helices (bars) and β-strands (arrows) are from the NMR-derived structure of Cdc4p (PDB entry 1GGW). Identical and similar residues are highlighted in black and gray, respectively. (B) Schematics of the constructs studied. The N-terminal Met1 is posttranslationally removed from Cdc4p. (C) Similar patterns of $^1H^\alpha$ secondary chemical shifts ($\delta_{obs} - \delta_{ref}$) are observed for corresponding residues in the isolated C-domains (Cdc4p-C, Cdc4-Cs) as in Cdc4p, indicating similar secondary structures. Note that upfield ($\Delta\delta < 0$) and downfield ($\Delta\delta > 0$) shifted $^1H^\alpha$ signals are diagnostic of α-helices and β-strands, respectively (*75*). This conclusion is confirmed by NOE patterns between main chain protons (not shown).

separated by a flexible linker (Figure 1A) (*23*). In contrast to many EF-hand proteins, yet similar to skeletal muscle ELC (*21*, *24*, *25*), purified Cdc4p does not bind calcium (*23*), and the mechanism for its regulation is still unknown. The existence of two domains connected by a flexible linker in Cdc4p raises questions about their structural and functional independence. In addition to binding Myo2p and Myp2p, two-hybrid screens revealed that only the C-domain of Cdc4p is required for interaction with a phosphatidylinositol (PI) 4-kinase, whereas both the N- and C-domains are needed for binding Vps27p, a zinc-finger domain protein implicated in vacuolar and endocytic membrane traffic (*26*−*28*). There is also evidence that Cdc4p interacts with Rng2p, an IQGAP protein, and with Myo5p, a type V myosin (*11*, *29*). Recently, Terrak et al. determined the crystal structures of *Saccharomyces cerevisiae* Mlc1p, an orthologue of Cdc4p, bound to peptides corresponding to the neck region of the Myo2p from this yeast (*30*). Interestingly, the Mlc1p bound different IQ motifs of Myo2p in two distinct modes, one involving only its C-domain and the other using both N- and C-domains (*30*).

With the goal of characterizing the structure, dynamics, and binding properties of the domains of Cdc4p, genes encoding each were cloned and expressed separately, yielding fragments denoted as Cdc4p-N and Cdc4p-C (Figure 1B). The structure and fast time scale backbone dynamics of isolated Cdc4p-N resemble closely those of the N-domain in Cdc4p, yet surprisingly, its stability is higher as judged by amide hydrogen-exchange measurements. On the other hand, the stability, structure, and fast time scale dynamics of isolated Cdc4p-C are all different from those of the C-domain in Cdc4p. In particular, properties of the isolated C-domain are dependent upon its precise N-terminal sequence due to intramolecular binding of this residual linker. Our results demonstrate that the C-domain of Cdc4p is both more structurally plastic and conformationally dynamic, as well as less thermodynamically stable, than the N-domain of this ELC. We hypothesize that these properties may allow Cdc4p to interact differentially via each domain with several regulatory or contractile ring proteins necessary for cytokinesis.

EXPERIMENTAL PROCEDURES

Cloning. A *cdc4* cDNA construct in the *Escherichia coli* expression vector pRSET B (Invitrogen) was a gift of Dr. Dan McCollum (Vanderbilt University). The genes encoding full-length Cdc4p (accession number Q09196, residues 1−141), its N-terminal domain (Cdc4p-N, residues 1−75), and its C-terminal domain (Cdc4p-C, residues 72−141) were subcloned by PCR methods into pET28a expression vector (Novagen). The plasmid also encodes an N-terminal His_6 tag with a thrombin cleavage site such that three extra amino acids (Gly-Ser-His) remain after removal of the tag (Figure 1B). The clones were verified by DNA sequencing.

Protein Expression and Purification. The expression and purification of Cdc4p, lacking a His_6 tag, have been described previously (*23*). This protein was used for NMR relaxation and thermal denaturation studies. In the cases of the pET28a-encoded proteins, freshly transformed *E. coli* BL21(λDE3) cells were grown overnight in 25 mL of Luria broth, collected by centrifugation, and transferred to 1 L of Luria broth for unlabeled proteins or minimal M9 medium containing 1 g of (99%) $^{15}NH_4Cl$ (Spectral Stable Isotopes) for uniform ^{15}N labeling. When cells reached an OD_{600} of ∼0.6, protein expression was induced with 1 mM IPTG. Cells were then grown overnight at 30 °C, harvested by centrifugation, and frozen at −70 °C prior to further purification.

Thawed *E. coli* pellets were resuspended in binding buffer (5 mM imidazole, 50 mM HEPES, 500 mM NaCl, 5% (v/v) glycerol, pH 7.5) and lysed by passage through a French press (1000 psi) followed by sonication (duty cycle ∼50%, 10 min). After centrifugation at 15000 rpm for 30 min, the supernatant was passed through a 0.8 μm filter (Millex) and applied to a 5 mL Hi-Trap metal affinity column (Amersham Biosciences). The column was washed with 200 mL of washing buffer (binding buffer plus 60 mM imidazole), and the His_6-tagged proteins were eluted with elution buffer (binding buffer plus 250 mM imidazole). Fractions containing the protein were pooled and placed in 2K MWCO dialysis tubing. The His_6 tag was removed by incubation with thrombin (∼0.5 mg, Roche) during overnight dialysis at 4 °C into NMR buffer (30 mM potassium phosphate, 100 mM KCl, 2 mM DTT, 0.1 mM EDTA, pH 6.5). After 48 h, the reaction was terminated by incubation with 100 μL of *p*-aminobenzamidine beads (Sigma) for 1 h. The supernatant was applied to the 5 mL Hi-Trap column to remove the

cleaved tag and any uncleaved protein. The samples were concentrated using a 1K MWCO filter (Pall Filtron) in an Amicon stirred cell concentrator under N_2 gas and stored at 4 °C. Cdc4p-C used for ATCUN-copper binding was dialyzed into NMR buffer without EDTA and DTT. In each case, the protein purity was judged to be >95% by SDS−PAGE, and the protein identity was confirmed by ESI-MS. The observed (predicted) masses, in daltons, of the ^{15}N-labeled proteins were 15706 (15707.5) for Cdc4p without an N-terminal Met, 16126 (16125.9) for Cdc4p with a residual N-terminal Gly-Ser-His, 8670 (8669.5) for Cdc4p-N, and 8165 (8165.2) for Cdc4p-C. Protein concentrations were determined by UV light absorption spectroscopy using predicted ϵ_{278} values (*31*) of 4200 M^{-1} cm^{-1} for Cdc4p, 1400 M^{-1} cm^{-1} for Cdc4p-N, and 2800 M^{-1} cm^{-1} for Cdc4p-C.

Cleavage by Acid Hydrolysis. Acid hydrolysis, which cleaves the Cdc4p linker between Asp75 and Pro76 (*32*), was used to produce a further truncated fragment of the C-domain (Cdc4p-Cs), comprising residues 76−141. A sample of ^{15}N-labeled His_6-tagged Cdc4p, prepared as described above, but not subjected to thrombin digestion, was diluted to 8.5 mg/mL in 75% (v/v) formic acid. The sample was incubated at 37 °C for 48 h, dialyzed exhaustively in binding buffer at 4 °C, and passed through a Hi-Trap metal affinity column to remove any uncleaved Cdc4p and the cleaved N-domain. The resulting Cdc4p-Cs from the flow-through was purified further by HPLC on a C_{18} reverse-phase column (Vydac, 25 × 10 cm, 20 mL bed volume) using a water/acetonitrile gradient with 0.1% trifluoroacetic acid. After lyophilization, the sample was dissolved in NMR buffer. The ^{15}N-labeled Cdc4p-Cs was judged to be >90% pure by SDS−PAGE and ESI-MS, with an observed (predicted) mass of 7478 (7474.4) Da.

Thermal Unfolding. Thermal unfolding measurements were monitored by CD spectropolarimetry using a Jasco 810 spectropolarimeter equipped with a PRF-452S Pelletier thermal control. All proteins were purified further by HPLC on a C_{18} reverse-phase column (Vydac, 25 × 10 cm, 20 mL bed volume), eluting at 60−65% acetonitrile/water in 0.1% trifluoroacetic acid. Pooled fractions were lyophilized, reconstituted in distilled water, and dialyzed overnight at 4 °C into NMR buffer. Samples (~15 μM final) were placed in a 0.2 cm quartz cell and thermal denaturation curves recorded by monitoring the signal at 222 nm as a function of temperature, increased at a rate of 1 °C/min. Reversibility was confirmed by the observation of similar CD spectra at 5 °C recorded before and after heating. T_m and ΔH°_{vh} values were obtained by fitting the resulting data to a two-state model (*33*, *34*).

NMR Spectral Assignments. Spectra were recorded at 30 °C using Varian Unity 500 MHz and Inova 600 MHz spectrometers. Unless stated otherwise, all samples were in NMR buffer with ~5% D_2O added for the lock signal. NMR data were processed using NMRpipe (*35*) and analyzed by SPARKY (*36*). Spectral assignments of full-length Cdc4p were reported previously (*23*). The ^{1}H−^{15}N HSQC spectrum of the untagged protein overlapped exactly with that of the protein with the cleaved His_6 tag, indicating that the additional four N-terminal residues (Gly-Ser-His-Met) did not perturb the structure of Cdc4p. ^{1}H and ^{15}N resonance assignments for Cdc4p-N, Cdc4p-C, and Cdc4p-Cs were obtained from 3D ^{15}N-edited TOCSY- and NOESY-HSQC experiments.

NMR Relaxation Measurements. Amide ^{15}N relaxation parameters were acquired at a proton frequency of 500 MHz as described by Farrow et al. (*37*). Steady-state heteronuclear $\{^1H\}^{15}N$-NOE spectra were recorded with and without 3 s of ^{1}H saturation and a total recycle delay of 5.017 s. Relaxation rates and correlation times were calculated using Curvefit (*38*) and Tensor2 (*39*), respectively.

Amide Proton−Deuterium Exchange. After recording reference ^{1}H−^{15}N HSQC spectra, ^{15}N-labeled Cdc4p, Cdc4p-N, and Cdc4p-C (~1 mM) in 500 μL of protonated NMR buffer were lyophilized and redissolved in an equivalent volume of D_2O. Amide exchange rates were measured by recording a series of sensitivity-enhanced ^{1}H−^{15}N HSQC spectra at 30 °C, starting ~5 min after the addition of D_2O. Initial spectra were obtained with a small number of scans to detect the exchange of the least protected residues, while later spectra were recorded with a greater number of scans for improved signal-to-noise ratio. Spectra were scaled according to the acquisition time and residue-specific exchange rates, k_{ex}, determined by fitting peak heights, $I_{(t)}$, to the equation $I_{(t)} = I_0 e^{-(k_{ex})t} + I_\infty$, where I_∞ is the baseline value, close to zero, due to residual protonated water. The pH* values after exchange were 6.7 ± 0.1 for all of the proteins. Control experiments using H_2O buffer demonstrated that each protein retains its folded structure after rehydration.

Protection factors (k_{rc}/k_{ex}) were derived from the predicted exchange rates (k_{rc}) for a random coil polypeptide with the sequence of Cdc4p. These rates were calculated with the program SPHERE using poly(D,L-alanine) reference data corrected for amino acid type, pH, temperature, and isotope effects (*40*, *41*).

Paramagnetic Relaxation. The titration of the ATCUN motif in Cdc4p-C (500 μL, 100 μM) with aliquots of 500 μM $CuSO_4$ in NMR buffer without EDTA and DTT was monitored using ^{1}H−^{15}N HSQC spectroscopy. Amide resonance assignments for the final 1:1 complex were confirmed from 3D ^{15}N-edited TOCSY- and NOESY-HSQC spectra. The effective distances from the paramagnetic center to selected amide protons were calculated as described previously (*42*), using paramagnetic relaxation enhancements derived from proton line width changes and an average global correlation time of 4.1 ns for Cdc4p-C.

Peptide Binding. A peptide corresponding to IQ1 (residues 775−795) of Myp2p (NSFSARIRGFLTRRRLYRFNHW, IQ motif underlined) was synthesized on a Rainin Symphony automated peptide synthesizer and purified by reverse-phase HPLC. An amidated Trp residue was appended to the C-terminus of Myp2p IQ1 for quantitation purposes. The peptide mass was verified by MALDI-MS and quantitated by absorbance using a predicted ϵ_{280} = 6970 M^{-1} cm^{-1}. The lyophilized peptide was dissolved in NMR buffer, and aliquots were added to 500 μL solutions of ~100 μM ^{15}N-labeled Cdc4p, Cdc4p-C, and Cdc4p-Cs. Saturation of binding was determined by monitoring each titration point with a ^{1}H−^{15}N HSQC spectrum.

RESULTS

The Isolated Domains Are Folded and Retain the Secondary Structure of Full-Length Cdc4p. The ^{1}H−^{15}N HSQC

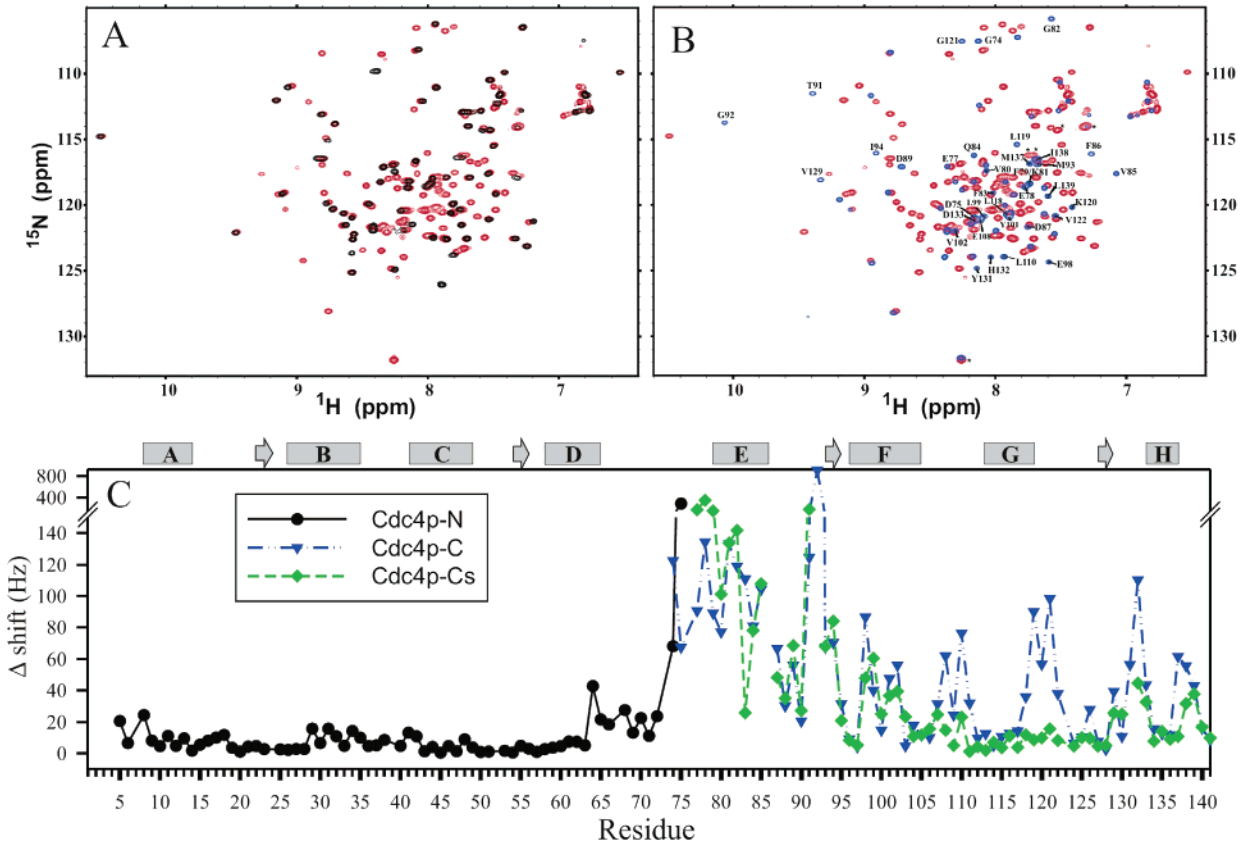

FIGURE 2: Superimposition of the ^{1}H−^{15}N HSQC spectra of (A) Cdc4p-N (black) and (B) Cdc4p-C (blue) onto that of Cdc4p (red). Main chain amide assignments are for residues of Cdc4p-C showing a chemical shift perturbation with respect to Cdc4p greater than 35 Hz. Aliased peaks are marked (*). (C) Changes in the amide chemical shifts of corresponding residues in the isolated domains [(●) Cdc4p-N, (▼) Cdc4p-C, and (◆) Cdcp4-Cs] versus full-length Cdc4p, calculated as $[(\Delta\upsilon_{^1H})^2 + (\Delta\upsilon_{^{15}N})^2]^{1/2}$ with data recorded on a 500 MHz NMR spectrometer. The secondary structure elements of Cdc4p are shown (α-helices, bars; β-strands, arrows). The excellent overlap between the spectra of Cdc4p and Cdc4p-N indicates that the N-domain has the same secondary and tertiary structures in isolation and in the native protein, whereas the poor overlap between parts of the spectra of Cdc4p and Cdc4p-C indicates a perturbation in the tertiary structure of Cdc4p-C.

spectra of Cdc4p and its isolated domains, Cdc4p-N, Cdc4p-C, and Cdc4p-Cs, recorded under identical experimental conditions are shown in Figure 2 (and Supporting Information, Figure S1). As evident by the good dispersion of these HSQC spectra, the individual domains adopt well-folded structures when separated. From ^{15}N-NOESY-HSQC spectra, similar patterns of sequential, short-range, and cross-strand NOE interactions between $^{1}H^{N}$, $^{1}H^{\alpha}$, and $^{1}H^{\beta}$ protons were found for corresponding residues in Cdc4p and its isolated domains (data not shown). Therefore, Cdc4p-N, Cdc4p-C, and Cdc4p-Cs retain similar α-helix and β-strand secondary structures as in native Cdc4p. This conclusion is supported by a comparison of the $^{1}H^{\alpha}$ secondary chemical shift patterns for Cdc4p, Cdc4p-C, and Cdc4p-Cs (Figure 1C).

The Tertiary Structure of the Isolated C-Domain Is Perturbed Relative to Full-Length Cdc4p. Chemical shift differences between corresponding amides in the full-length protein and each domain are plotted in Figure 2C. With the exception of signals arising from the cleaved linker, peaks in the spectrum of Cdc4p-N superimpose almost exactly with the corresponding signals in the spectrum of Cdc4p. Given the exquisite sensitivity of the ^{1}H and ^{15}N chemical shifts of an amide to its environment, this clearly demonstrates that the N-domain retains the same secondary and tertiary structure whether in isolation or in the context of the full-length protein. In contrast, resonances from amides throughout Cdc4p-C and Cdc4p-Cs are significantly altered relative to Cdc4p, indicative of structural perturbations. Since their secondary structures are retained, the differences in the ^{1}H−^{15}N HSQC spectra between native Cdc4p and the isolated C-domain fragments must reflect conformational changes at the tertiary structural level.

The observation that the structure of the C-domain, but not N-domain, changes upon its isolation is surprising, as one would have expected neither domain to be perturbed if they behave as "beads on a string" or both to be perturbed if they interact in the context of native Cdc4p. To probe for possible interactions between the isolated domains of Cdc4p, ^{1}H−^{15}N HSQC spectra of ^{15}N-labeled Cdc4p-C or Cdc4p-N (∼130 μM) were recorded in the absence and presence of a 10-fold molar excess of unlabeled Cdc4p-N or Cdc4p-C, respectively. No significant spectral changes were observed in either case, indicating that the two separate domains do not interact with any measurable affinity (data not shown). This prompted us to examine the effects of the N-terminal residues remaining from the cleaved linker.

Previous NMR spectroscopic studies of Cdc4p (*23*) demonstrated that the N-domain and C-domain are connected by a flexible proline-rich linker (^{65}NRPNGFDMPGDPEE^{78}, Figure 1B). We initially reasoned that cleavage at Met72, near the center of the linker, would leave seven unstructured residues, plus a Gly-Ser-His tripeptide from the His_6 tag, preceding the C-domain, and thus should avoid the introduction of any non-native effects such as a new positively

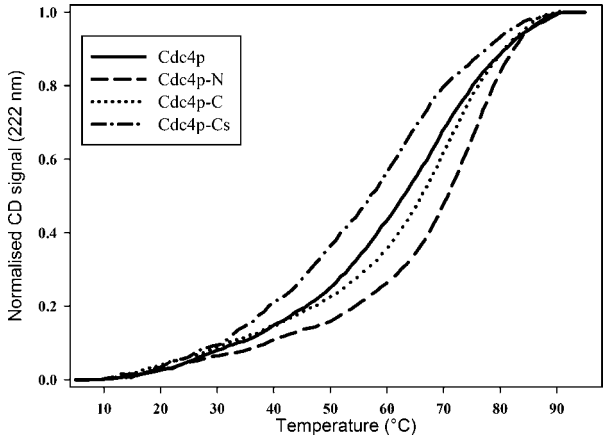

FIGURE 3: Thermal denaturation of Cdc4p (—), Cdc4p-N (− −), Cdc4p-C (···), and Cdc4p-Cs (− · −) at pH 6.5 monitored by CD spectropolarimetry demonstrates that the isolated N-domain is more stable than the isolated C-domain and that stability of the C-domain is dependent upon the residual linker sequence. The displayed data were smoothed with a running average function and then normalized to the respective end points. The raw data were fit (*34*), yielding the following parameters: Cdc4p, T_m (apparent) = 67 °C; Cdc4p-N, T_m = 74 °C, ΔH°_{vh} = 45.4 kcal mol^{-1}; Cdc4p-C, T_m = 71 °C, ΔH°_{vh} = 38.2 kcal mol^{-1}; and Cdc4p-Cs, T_m = 60 °C, ΔH°_{vh} = 23.9 kcal mol^{-1}. The van't Hoff enthalpy for Cdc4p was not determined because its denaturation profile represents the contributions of its two constituent domains.

charged amino group immediately adjacent to the domain (Figure 1). Indeed, on the basis of the lack of medium/long-range NOE interactions (data not shown), the residual linker of Cdc4p-C appears to be predominantly unstructured. Nevertheless, to test this assumption, we subsequently used acid hydrolysis to selectively cleave Cdc4p between Asp75 and Pro76 and thereby remove the Gly-Ser-His extension as well as residues 72−75. With the exception of the first ~10 N-terminal residues, the chemical shifts of corresponding amides in the ^{1}H−^{15}N HSQC spectrum of the truncated construct, Cdc4p-Cs, appeared to be intermediate between those of Cdc4p and Cdc4p-C (Figure 2C and Supporting Information, Figure S1). Thus the spectral, and hence structural, perturbations of the C-domain depend on the nature of the preceding linker sequence.

Thermal Denaturation Studies Reveal That Cdc4p-N Is More Stable Than the Cdc4p-C. CD spectropolarimetry was used to monitor the temperature-dependent unfolding transition of Cdc4p and its isolated domains (Figure 3). Cdc4p reversibly unfolds with an apparent midpoint T_m of 67 °C at pH 6.5. The transitions corresponding to unfolding of the individual domains could not be resolved. Surprisingly, upon cleavage of its linker, the T_m values of both isolated domains increased, with Cdc4p-N having the highest T_m of 74 °C and Cdc4p-C an intermediate value of 71 °C. However, further truncation of the linker to produce Cdc4p-Cs significantly lowered the stability of the C-domain, as reflected by a T_m of 60 °C. Consistent with ^{1}H−^{15}N HSQC spectral comparisons, the properties of the C-domain are dependent upon the residues at its N-terminus.

The C-Domain Shows Less Protection from Amide Hydrogen Exchange Than the N-Domain. Amide proton−deuterium exchange (HX) experiments were used to probe the stability and dynamics of the domains of Cdc4p in isolation and in their native context. In addition to the known effects of sequence, the exchange rate of a specific amide

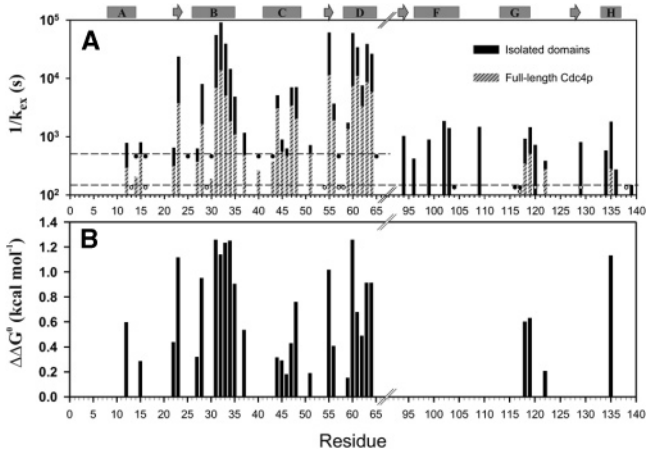

FIGURE 4: Amide proton−deuterium exchange reveals that Cdc4p-N is more stable than Cdc4p-C, and both are more stable in isolation than when linked together in Cdc4p. (A) HX lifetimes for Cdc4p (hatched bars) and Cdc4p-N and Cdc4p-C (solid bars) at pH 6.5 and 30 °C. The dashed horizontal lines show the minimum lifetimes that could be measured under the experimental conditions for Cdc4p and Cdc4p-C (lower line) and Cdc4p-N (upper line). The initial spectra of Cdc4p and Cdc4p-C were acquired faster than the initial spectra of the slower exchanging Cdc4p-N, giving the difference in these lower limits. Dots indicate residues for which a signal was detected only in the first spectrum recorded for each protein, thus precluding a reliable measurement of k_{ex}. Filled and empty dots correspond to residues in Cdc4p and the isolated domains, respectively. Missing data are for prolines, residues with no detectable signal in the first spectra recorded (i.e., linker and helix E), or residues with overlapping signals. (B) Difference in free energies, $\Delta\Delta G^\circ = -RT \ln(k_{ex,domain}/k_{ex,Cdc4p})$, associated with the conformational equilibria between closed and open exchange states for each residue in the isolated domains compared with those in Cdc4p.

hydrogen in a protein is dependent upon its structural environment, including hydrogen bonding and solvent accessibility, as well as local and global fluctuations leading to water contact (*43*). The measured exchange lifetimes ($1/k_{ex}$) of Cdc4p, Cdc4p-N, and Cdc4p-C reveal three striking conclusions (Figure 4). First, whether in isolation or in the full-length protein, amides within the N-domain exchange on the order of 10−100-fold slower than those in the C-domain. Second, amides in Cdc4p-N and Cdc4p-C have lifetimes 1.5−10 times longer than the corresponding amides in Cdc4p. Third, in all cases, the linker residues, as well as helix E of the C-terminal domain, exchange within the deadtime of the experiment (~2 min), indicative of significant solvent accessibility and/or conformational mobility.

Under EX2 conditions, protection factors can be interpreted as the inverse of an equilibrium constant for fluctuations between a closed nonexchangeable state and a transiently open exchange-competent state (*43*). Thus protection factors provide a measure of residue-specific free energy changes, $\Delta G^\circ_{HX} = RT \ln(k_{rc}/k_{ex})$, governing local and global conformation dynamics allowing exchange. On the basis of the largest protection factors measured for the N-domain in Cdc4p-N (Phe60, 2.8×10^5) and in Cdc4p (Phe60, 4.4×10^4), the minimum estimates of the free energy changes for global unfolding of this domain under native conditions are 7.5 kcal/mol in isolation and 6.4 kcal/mol in the native protein. Similarly, from the largest protection factors for the C-domain in Cdc4p-C (Lys109, 6.9×10^3) and in Cdc4p (Leu119, 5.4×10^2), the minimum estimated free energy changes for unfolding of this domain are 5.3 kcal/mol in

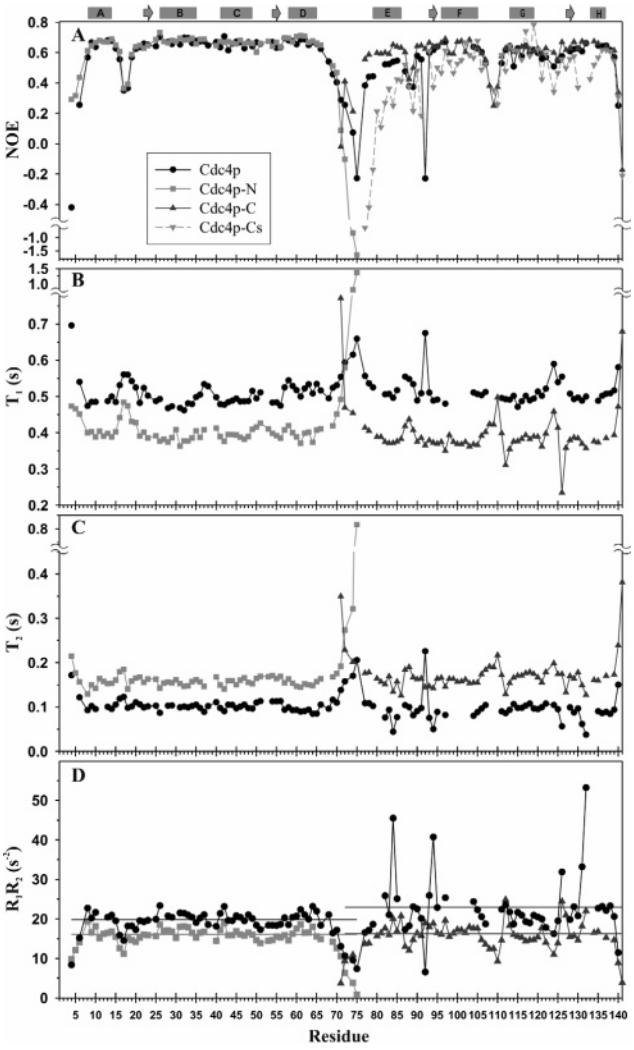

FIGURE 5: Global and local backbone dynamics of Cdc4p (●), Cdc4p-N (■), Cdc4p-C (▲), and Cdc4p-Cs (▼) probed by amide ^{15}N relaxation. Data were collected at 30 °C and pH 6.5 using a 500 MHz spectrometer. Missing points correspond to prolines or residues with overlapping or anomalously weak signals. (A) Heteronuclear {^{1}H}^{15}N-NOE values of Cdc4p reveal that the fast time scale dynamics of amides 77−93, which include helix E, as well as Gly92, are dependent upon the residues N-terminal to the C-domain. Errors are 2% for Cdc4p and Cdc4p-C and 18% for Cdc4p-Cs, with the latter reflecting the reduced concentration of the acid-cleaved protein available for these studies. Based on ^{15}N (B) T_1 and (C) T_2 relaxation data, (D) the products of the amide R_1 ($=1/T_1$) and R_2 ($=1/T_2$) relaxation rates were calculated, with average values for each domain indicated by the horizontal lines. Anomalously low R_1R_2 values are indicative of enhanced mobility on a nanosecond to picosecond time scale, whereas high values reveal a contribution of millisecond to microsecond conformational exchange broadening, R_{ex}, to the amide ^{15}N transverse relaxation. With the exception of mobile loop regions, residues in Cdc4p-N and the N-domain of Cdc4p show relatively uniform R_1R_2 values. In contrast, several residues in the C-domain of Cdc4p (Gln84, Ile94, Asp126, Tyr131, and His132) exhibit high R_1R_2 values, indicative of exchange broadening. Such behavior is less pronounced in the isolated Cdc4p-C.

isolation and 3.8 kcal/mol in Cdc4p. Thus, Cdc4p-N is more stable against HX than Cdc4p-C, and both are more stable in isolation than in the intact protein under native conditions.

NMR Relaxation Highlights the Context-Dependent Dynamics of the C-Domain. The dynamic properties of Cdc4p and its isolated domains were investigated using amide ^{15}N relaxation experiments (Figure 5). From the measured T_1 and T_2 values, summarized in Table 1, the effective correlation times for the global tumbling of Cdc4p-N and Cdc4p-C are 4.6 and 4.1 ns, respectively. These values are consistent with those expected for monomeric proteins having the molecular mass of Cdc4p-N (8.7 kDa) and Cdc4p-C (8.2 kDa) (*44*). The longer T_1 and shorter T_2 times measured for Cdc4p reflect the higher molecular weight and hence slower tumbling of this full-length protein.

In addition to providing a measure of the global rotational diffusion of a protein, ^{15}N relaxation data reflect the local mobility of its polypeptide backbone on a residue-specific basis. In general, reduced {^{1}H}^{15}N-NOE values and elevated T_2 lifetimes indicate enhanced flexibility on a nanosecond to picosecond time scale, whereas short T_2 lifetimes arise from conformational exchange broadening on a millisecond to microsecond time scale. Although motional anisotropy may also lead to local, structure-dependent variations in the measured relaxation parameters, these effects are attenuated by consideration of the product R_1R_2 [$=1/(T_1T_2)$]. Specifically, low R_1R_2 values reflect residues with enhanced fast time scale mobility, whereas high values serve to distinguish those residues undergoing conformational exchange broadening (*45*). For example, flexibility on the nanosecond to picosecond time scale for the linker, termini, and loops (i.e., between helixes A and B) of Cdc4p is evident from the relaxation data presented in Figure 5. This behavior has been discussed previously in terms of the structure of Cdc4p (*23*).

Focusing on a comparison of Cdc4p with the isolated domains, the relaxation parameters measured for Cdc4p-N closely mirror those of the corresponding residues in Cdc4p. In combination with HSQC spectral comparisons, these data indicate that neither the structure nor fast time scale dynamics of the N-domain are perturbed upon its isolation. Although the ^{15}N relaxation of Cdc4p-C overall resembles that of the C-domain of Cdc4p, several notable differences can be seen in Figure 5 and in Table 1. First, Gly92 appears unusually dynamic in Cdc4p, with a ^{1}H{^{15}N}-NOE value of −0.2, whereas in Cdc4p-C its relaxation behavior is similar to that of its neighboring amides. The role of this residue in peptide binding will be discussed below. Second, several residues of the C-domain of Cdc4p exhibit anomalously high R_1R_2 values, whereas the N-domain of Cdc4p, Cdc4p-N, and Cdc4p-C show more uniform relaxation parameters (Figure 5D). Thus, ^{15}N relaxation data indicate the occurrence of millisecond to microsecond motions in the C-domain of Cdc4p that are absent in the N-domain and in isolated Cdc4p-C. Third, although the initial N-terminal linker residues of Cdc4p-C are clearly flexible, amides 77−93 (helix E and the preceding two linker residues) have higher ^{1}H{^{15}N}-NOE values than in Cdc4p, indicative of more restricted motion on the nanosecond to picosecond time scale. This behavior is unexpected as these residues are no longer tethered to the N-domain of Cdc4p and, if anything, should show increased mobility. Indeed, upon further truncation to produce Cdc4p-Cs, the ^{1}H{^{15}N}-NOE values of residues 77−85 become markedly reduced relative to both Cdc4p and Cdc4p-C, indicating such increased flexibility (Figure 5A). As shown below, these differences are explained by the cleaved linker region binding intramolecularly to the remainder of Cdc4p-C.

The Chemical Shifts of Thr91 and Gly92 Are Indicators of the Peptide-Bound Conformation of the C-Domain. The

Table 1: ^{15}N Relaxation Data for Cdc4p and Its Isolated Domains

	T_1 (ms)[a]	T_2 (ms)[a]	R_1R_2 (s^{-2})[a]	NOE[a]	τ_c (ns)[b]
N-domain in Cdc4p	503 ± 25	101 ± 8	19.9 ± 1.8	0.63 ± 0.07	7.6 ± 0.1[c]
C-domain in Cdc4p	512 ± 34	91 ± 27	23.1 ± 7.7	0.56 ± 0.14	8.1 ± 0.1[c]
Cdc4p-N	403 ± 26	158 ± 11	15.9 ± 1.7	0.64 ± 0.09	4.6 ± 0.1
Cdc4p-C	382 ± 34	164 ± 18	16.4 ± 2.9	0.61 ± 0.08	4.1 ± 0.1

[a] Average (±standard deviation) values, excluding highly mobile amides from N- and C-termini. [b] The effective correlation time (τ_c) for global tumbling was calculated for each domain excluding amides exhibiting anomalous T_1/T_2 ratios or low ^{1}H{^{15}N}-NOE values indicative of enhanced internal mobility. [c] Each domain was fit separately due to the dumbbell shape of Cdc4p and the presence of a flexible linker.

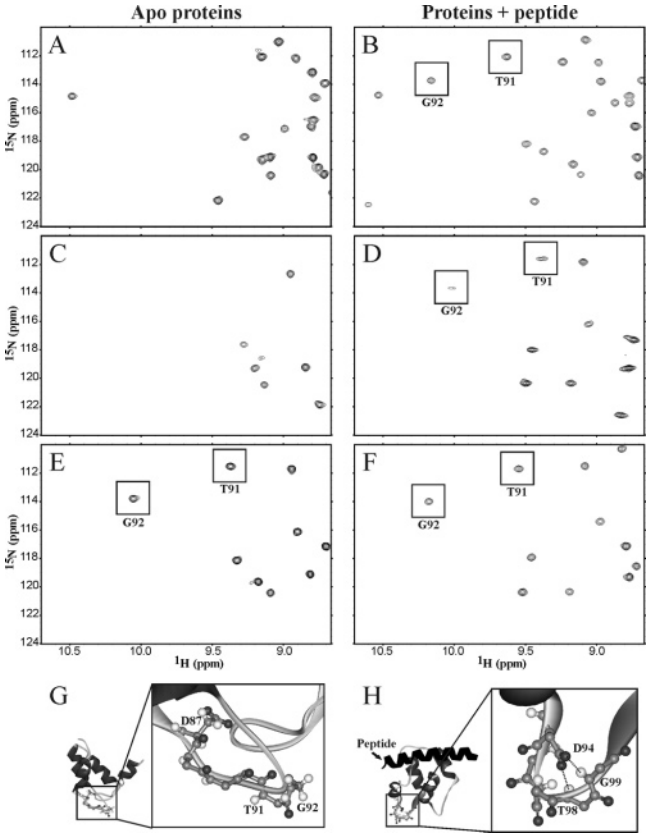

FIGURE 6: The downfield chemical shifts of Thr91 and Gly92 (boxed) are diagnostic of a peptide-bound conformation of the C-domain. The left column shows portions of the ^{1}H−^{15}N HSQC spectra of the apoproteins, and the right column shows the same proteins bound to the Myp2 IQ1 peptide for Cdc4p (A, B), Cdc4p-Cs (C, D), and Cdc4p-C (E, F). (G) Structure of the C-domain in apo-Cdc4p (PDB entry 1GGW). The amides of Thr91 and Gly92 are distant from the side chain of Asp87. (H) Structure of peptide-bound Mlc1p (PDB entry 1M46). The nitrogen atoms of the amides of Thr98 and Gly99, equivalent to residues 91 and 92 in Cdc4p, are both positioned ∼2.8 Å from the side chain oxygen atoms Asp94. These hydrogen bonds are likely responsible for the downfield ^{1}H^N shifts of Thr91 and Gly92 upon peptide binding by Cdc4p and Cdc4p-Cs. Surprisingly, free Cdc4p-C shows these downfield-shifted peaks in the absence of added peptide, indicating intramolecular binding to the residues from the cleaved linker sequence.

most pronounced differences between the NMR spectra of Cdc4p-C and the C-domain of Cdc4p lie with the ^{1}H^N chemical shifts of Thr91 and Gly92 (Figure 2C). For example, the signal from Gly92 is at 8.33 ppm in Cdc4p, yet at 10.06 ppm in Cdc4p-C (Figure 6). Remarkably, upon binding a peptide corresponding to the first IQ motif of Myp2p, the ^{1}H^N resonance from Gly92 in Cdc4p shifts dramatically downfield to 10.16 ppm, whereas in Cdc4p-C it only moves to 10.11 ppm. Similar to Cdc4p, when the peptide Myp2p IQ1 is added to Cdc4p-Cs, a clear signal for Gly92 appears at 9.95 ppm (Figure 6D). Such dramatic chemical shift changes in Thr91 and Gly92 can be rationalized by examining the available structures of apo-Cdc4p (*23*) and peptide-bound Mlc1p (*30*). In the former, the amide nitrogens of Thr91 and Gly92 are ∼9 and ∼8 Å away from the side chain carboxyl of Asp87, respectively (Figure 6G), whereas in the latter, the corresponding Thr98 and Gly99 are both ∼2.8 Å from the side chain of Asp94 (Figure 6H). This suggests that, upon peptide binding, the conformation of the Cdc4p C-domain changes, leading to formation of this hydrogen bond network, as evident by the downfield-shifted resonances of these two amides, as well as the increased ^{1}H-{^{15}N}-NOE value of Gly92. The observation of such a spectral signature for apo-Cdc4p-C led us to hypothesize that the residual linker sequence is bound intramolecularly in a manner comparable to the intermolecular binding of an IQ-motif peptide. This hypothesis is supported by paramagnetic relaxation enhancement studies.

Paramagnetic Relaxation Enhancement Confirms Intramolecular Linker Binding by Cdc4p-C. To investigate the position of the N-terminus of Cdc4p-C with respect to the remainder of the protein, we exploited the Gly-Ser-His tripeptide, remaining after thrombin cleavage of the His_6 tag, as an ATCUN motif (*46*). This motif binds Cu^{2+} with very high affinity ($K_D \approx 10^{-15}$ M), thereby providing a means to introduce a paramagnetic probe at a specific site in Cdc4p-C and obtain long-range distance restraints to backbone amide protons via relaxation enhancement NMR spectroscopy. In the case of an ordered ATCUN, proton−Cu^{2+} distances of ∼10−20 Å can be measured from enhanced ^{1}H relaxation (*47*). At distances less than this lower limit, signals are generally broadened beyond detection. However, mobility will attenuate the $1/r^6$-dependent effect, and thus we have used this approach primarily as a qualitative indicator of the proximity of an amide proton to the bound Cu^{2+} probe.

The relative changes in the ^{1}H−^{15}N HSQC peak intensity of each amide in Cdcp4-C in the absence and presence of a stoichiometric amount of Cu^{2+} are presented in Figure 7A (with spectra shown in Supporting Information, Figure S2). As expected, signals from amides near the N-terminus of Cdc4p-C were severely broadened due to paramagnetic relaxation enhancement from the adjacent ATCUN-bound metal. However, amides from residues 106−111, between helices F and G, and residues 134−141 at the C-terminus of the protein also showed weakened signals indicative of proximity to the metal ion. To estimate the location of the ATCUN motif in Cdc4p-C, the distances between the paramagnetic center Cu^{2+} and three representative amides, Glu77, Gly107, and Val135, were approximated from their ^{1}H^N relaxation enhancements. Triangulation from their counterparts in the peptide-bound Mlc1p structure revealed

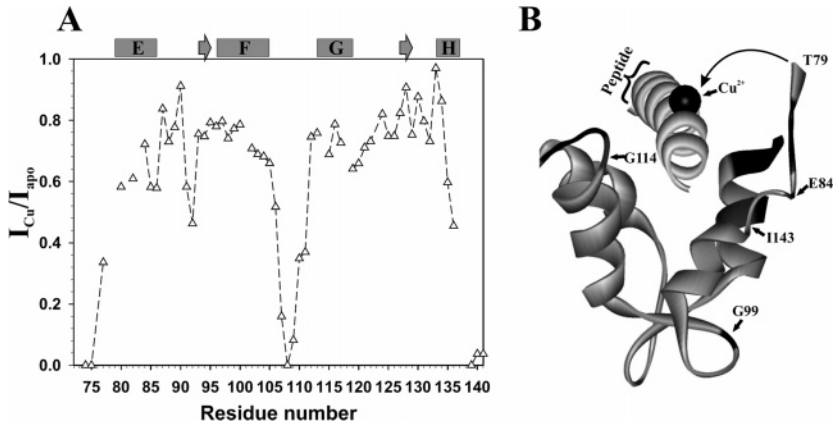

FIGURE 7: The N-terminal ATCUN motif (Gly-Ser-His) of Cdc4p-C is proximal to residues at its N- and C-termini and in the loop between its two EF-hands. (A) Relative $^1H-^{15}N$ HSQC peak intensities for a 1:1 Cdc4p-C:Cu^{2+} complex versus the metal-free protein. Paramagnetic relaxation enhancement due to proximity of an amide proton to the bound metal leads to a decrease in signal intensity beyond that of ~5/6 due to dilution of the sample (initially 500 μL) upon addition of $CuSO_4$ solution (100 μL). Missing data points correspond to prolines, residues with overlapping signals, or residues undetectable due to severe to line broadening. (B) Structure of the C-domain of Mlc1p, the *S. cerevisiae* orthologue of Cdc4p, bound to an IQ-motif peptide (PDB entry 1M46). Line broadening of representative amides in different parts of Cdc4p-C (Glu77, Gly107, and Val135) was used to calculate the approximate distances to the paramagnetic Cu^{2+}. Triangulating from the corresponding amides in Mlc1p (Glu84, Gly114, and Ile143) indicates that the ATCUN-bound Cu^{2+} (black ball) lies within the cleft of Cdc4p-C corresponding to that occupied by the bound peptide in the crystal structure of Mlc1p. This demonstrates that the residual linker at the N-terminus of Cdc4p-C is located within its peptide binding cleft (Thr79 in Mlc1p corresponds to Met72 in Cdc4p).

that the Cu^{2+} must lie within the peptide-binding cleft of Cdc4p (Figure 7). This strongly supports the hypothesis that the residual linker, including the ATCUN motif, is bound intramolecularly by Cdc4p-C. However, as evident by the low $^1H\{^{15}N\}$-NOE values of these N-terminal residues (Figure 5) and their lack of any predominant structure, this interaction may be transient, reflecting a conformational ensemble of a bound state(s) in equilibrium with a more dynamic unbound state(s).

DISCUSSION

Although several studies have stressed the importance of intact Cdc4p for cytokinesis, its exact roles in this process remain to be fully elucidated. Cdc4p binds to the actin−myosin contractile ring, but the observation of interallelic complementation between mutant forms of the protein, combined with the results of two hybrid screens and in vitro assays of myosin motility activity with Cdc4p mutants, indicates that its function extends beyond that of a simple ELC (*7*, *11*, *28*, *48*). In particular, Cdc4p also associates with other non-myosin proteins via one or both of its two domains (*28*). To provide a framework for understanding the molecular mechanisms by which Cdc4p functions in cytokinesis, we have characterized the structure, stability, and dynamics of its isolated N- and C-domains. Despite their 39% sequence similarity and conserved secondary structures, the properties of the two domains are very distinct. Most dramatically, the C-domain exhibits a high degree of conformational plasticity that is revealed by varying the cleaved linker sequence preceding this domain.

Spectral Perturbations Indicate Structural Plasticity of the C-Domain. Our studies demonstrate that the structure and fast dynamics of the N-domain do not change when it is cleaved from the C-domain. In contrast, the striking differences between the $^1H-^{15}N$ HSQC spectra of Cdc4p-C, Cdc4p-Cs, and Cdc4p indicate changes in the tertiary structure of the C-domain that are dependent upon the nature of the sequence preceding the domain. The structural perturbation of the isolated C-domain, but not N-domain, is unexpected. In general, with homologues of Cdc4p such as vertebrate calmodulin and caltractin, each domain is structurally independent as evident by superimposable NMR spectra with the full-length proteins (*49*−*52*). However, in the case of *S. cerevisiae* calmodulin, both isolated domains show structural changes when expressed separately from the full-length protein (*50*). These changes were attributed to interdomain interactions in the intact protein that were no longer possible when each domain was studied in isolation. In support of this argument, mixing of the two domains led to a heterodimeric complex ($K_D \sim 5-15$ mM) with an HSQC spectrum resembling that of the full-length calmodulin. However, using a similar approach, we were unable to detect any interdomain interactions between Cdc4p-C and Cdc4p-N. This indicates that the conformational changes exhibited by the C-domain, when isolated, are not due to absence of the N-domain. Furthermore, these results point to a plasticity of the C-domain that allows it to adopt different conformations that are dependent upon the precise linker sequence at its N-terminus.

The Structure of the C-Domain Is Context Dependent Due to Intramolecular Binding of the Linker Sequence. The structural perturbations observed for the C-domain of Cdc4p when isolated prompted us to investigate the effects of the residual linker preceding its folded structure. On the basis of our studies, we conclude that the residual linker, including possibly the Gly-Ser-His remaining after cleavage of the His_6 tag, is responsible for the structural perturbations of Cdc4p-C due to intramolecular binding in a mode similar to that for the intermolecular association of IQ-motif sequences. This conclusion is supported by three lines of evidence.

The first and most direct evidence comes from structural characterization of Cdc4p-C by Cu^{2+} paramagnetic relaxation measurements (*46*, *53*). Addition of Cu^{2+} to Cdc4p-C resulted in selective signal broadening and chemical shift perturbations for amides near its N-terminal ATCUN motif, as well as at positions 106−111 and 134−141. On the basis of

distances between selected amides and the bound Cu^{2+}, estimated from the observed paramagnetic relaxation enhancements, the approximate location of Cu^{2+} in Cdc4p was obtained. Remarkably, this location corresponds closely to the X-ray crystallographically determined position of an IQ-motif peptide within the binding cleft of Mlc1p (Figure 7). This result suggests strongly that the intramolecular association of the residual linker sequence by Cdc4p-C involves the same binding site as that used by the C-domain to intermolecularly associate with a myosin heavy chain.

The second line of evidence for intramolecular binding of the residual linker in Cdc4p-C is the presence of significantly downfield-shifted amide resonances for Thr91 and Gly92 in its $^1H-^{15}N$ HSQC spectrum. These signals are absent in apo-Cdc4p and -Cdc4p-Cs, yet appear upon binding to an IQ-motif peptide from Myp2p (Figure 6). The amide Gly92 is also conformationally mobile in Cdc4p, but not in Cdc4p-C, as evident by its $^1H\{^{15}N\}$-NOE values (Figure 5). NMR signals from deshielded glycine amide protons have been observed in many EF-hand proteins such as Ca^{2+}-loaded calmodulin, rabbit skeletal troponin C (*54*), pike parvalbumin (*55*), and caltractin (*49*, *56*), among others. Their unusual $^1H^N$ chemical shifts are diagnostic of a hydrogen bond with the side chain of an aspartate within a loop linking the two helices of the EF-hand motif (*57*, *58*). Interestingly, Thr91 and Gly92 are far from the IQ-motif binding site of the C-domain (see Gly99 in Figure 7B), indicating that the formation of the hydrogen bonds to Asp87 must result from an overall change in the tertiary conformation of the C-domain accompanying peptide binding.

The third piece of evidence for intramolecular binding in Cdc4p-C is seen from the effect of truncating its residual linker. Cdc4p-Cs lacks seven residues at the N-terminus of Cdc4p-C. With the exception of the flexible residues near helix E, which may be perturbed by the adjacent charged amino terminus, the $^1H-^{15}N$ amide shifts of Cdc4p-Cs resemble more closely those of Cdc4p than Cdc4p-C (Figure 2 and Supporting Information, Figure S1). This suggests that the much shorter residual linker can no longer interact with the C-domain, yielding a conformation closer to that of apo-Cdc4p.

The sequence of the residual linker ($GSH^{72}MPGDPEE^{78}$) is clearly different from the IQ motifs (IQxxxRGxxxR) in Myo2p and Myp2p that are recognized by Cdc4p. Therefore, there must be other factors that allow this sequence to associate with the peptide-binding cleft of Cdcp4-C. Most obviously, the residual linker is covalently attached to the C-domain, leading to intra- rather than intermolecular binding, a less entropically unfavorable event. That is, the covalent attachment leads to a high local concentration of the linker sequence, which greatly increases the propensity for binding, even if in a suboptimal fashion. This principle was clearly illustrated by Martin et al. (*59*) in studies of *Xenopus laevis* calmodulin covalently fused, through a highly flexible pentapeptide linker at its C-terminus, to a 24-residue target peptide. In this case, the enhanced intramolecular binding of the tethered peptide was reflected by an increased affinity for Ca^{2+}. Additionally, the plasticity of the C-domain could allow it to adopt different conformations to facilitate recognition of different target sequences. Note that this association may be relatively weak, as ^{15}N relaxation measurements indicate that the N-terminal residues in Cdcp4-C remain conformationally dynamic on a subnanosecond time scale (Figure 5). Fast HX rates and the lack of medium- and long-range homonuclear NOE interactions with the remainder of the C-domain are further evidence of the flexibility of the residual linker. It is also not readily clear why the C-domain binds the linker when isolated, yet not when it is attached to the N-domain in Cdc4p, since this region appears unstructured, and thus accessible, in the native protein (*23*). Most likely, steric hindrance from the folded N-domain prevents linker binding by the C-domain in full-length Cdc4p. Indeed, our HX data suggest that the C-domain binds either the linker or the N-domain when the latter is transiently unfolded (see below). Alternatively, the artificial N-terminal Gly-Ser-His or the positively charged amino-terminal group may contribute toward the intramolecular association of the residual linker in Cdc4p-C.

Non-native intramolecular association of a C-terminal EF-hand domain with its N-terminus has been previously reported for a construct of the calmodulin-like protein, centrin 2 (*56*). However, in that case, the N-terminal sequence was much longer (19 residues) and comprised all the residues of helix D, an amphipathic helix from the N-domain that, not surprisingly, interacted with the C-domain through hydrophobic interactions. In contrast, the N-terminal sequence of Cdc4p-C is much shorter and corresponds to an unstructured, flexible linker within the context of the native protein. Interestingly, different C-terminal extensions of the N-domain of *Paramecium* calmodulin have also been reported to alter its properties in the absence of the remaining C-domain (*60*). The alteration was attributed mainly to the stabilization of helix D by polar and charged residues, augmented by a few contacts between the C-terminal extension and helix A. The structural perturbations were smaller and more localized than what we observe in Cdc4p-C.

The C-Domain Is Less Stable Than the N-Domain. Understanding the conformational stability of proteins is key in the quest of discovering their function (*61*). Accordingly, we determined the stability of Cdc4p and its domains under both denaturing and native conditions using thermal unfolding and amide HX measurements, respectively. On the basis of T_m and ΔH°_{vh} values, the stabilities of the isolated domains against thermal unfolding follow the order of Cdc4p-N > Cdc4p-C > Cdc4p-Cs. The CD-monitored denaturation profile of Cdc4p could not be deconvoluted into distinct transitions for its N- and C-domains, thus precluding a comparison of their relative stabilities within the context of the full-length protein. In contrast, amide HX measurements by $^1H-^{15}N$ HSQC spectroscopy allowed us to measure the relative stabilities of the N- and C-domains, both in isolation and in Cdc4p, under native conditions. Assuming that most protected amides in a protein exchange via global fluctuations (*62*, *63*), ΔG°_{HX} values were calculated using the largest protection factor measured for each construct (Figure 8). Since exchange may also occur via local fluctuations, these values represent minimum estimates of the ΔG° for global unfolding of each species. The HX data clearly indicate that the stability of the constructs is Cdc4p-N > N-domain in full-length Cdc4p > Cdc4p-C > C-domain in full-length Cdc4p. Due to the low quantities of Cdc4p-Cs available, it was not practical to carry out HX studies on this truncated protein.

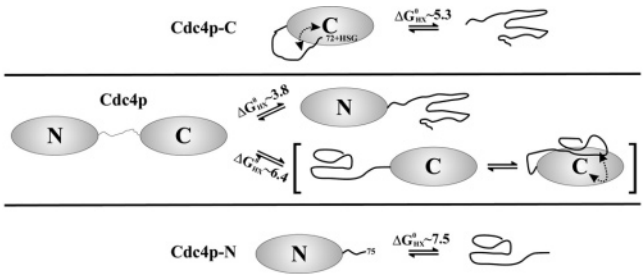

FIGURE 8: Schematic representations of the unfolding equilibria for Cdc4p, Cdc4p-N, and Cdc4p-C leading to HX under native conditions. The C-domain shows consistently lower ΔG°_{HX} values, in kcal mol^{-1}, than the N-domain, whether in isolation or in the full-length protein. The higher ΔG°_{HX} measured for Cdc4p-C relative to the C-domain of Cdc4p is attributed to the stabilization of its folded structure by the intramolecular binding of the residual linker sequence (dotted arrow). The lower ΔG°_{HX} of the N-domain in Cdc4p relative to that of Cdc4p-N may result from an intramolecular interaction between the transiently unfolded N-domain or linker with the folded C-domain of Cdc4p (dotted arrow).

The increased stability of the folded state of Cdc4p-C relative to Cdc4p-Cs and the C-domain in Cdc4p is attributed to the intramolecular binding of its residual linker sequence. In addition to favorable interactions between residues in the linker with those along the peptide-binding cleft of the C-domain, this association induces the formation of hydrogen bonds between the amides of Thr91 and Gly92 with the side chain of Asp87. On the basis of HX protection factors, linker binding by Cdc4p-C leads to a stabilization of ~1.5 kcal/mol at 30 °C. However, even with this contribution, the C-domain is consistently less stable than the N-domain, whether isolated or in Cdc4p.

Surprisingly, amide HX measurements indicate that the stability of the N-domain increases upon its isolation, despite having an unperturbed tertiary structure and fast time scale dynamics, as evident by invariant ^{1}H$-^{15}$N HSQC spectra and ^{1}H{^{15}N}-NOE values, respectively. On the basis of protection factors, Cdc4p-N is ~1.1 kcal/mol more stable than its counterpart in the full-length protein under native conditions. A plausible explanation for this observation is that a transiently unfolded, exchange-competent state of the N-domain in Cdc4p is stabilized by the binding of this domain and/or the linker sequence to the folded C-domain in a manner similar to that found for the association of Cdc4p-C with its residual N-terminal linker (Figure 8). Note that, in contrast to thermal unfolding studies where the less stable C-domain will be largely unfolded at the T_m of the N-domain, and thus unable to partake in such an interaction, under the native conditions used for HX measurements, fluctuations of each domain occur predominantly within the context of a folded neighboring domain. This interaction is reminiscent of that reported between the folded and unfolded domains of *Drosophila melanogaster* apo-calmodulin. Masino et al. discovered that the Ca^{2+}-free N-domain from calmodulin was ~0.8 kcal/mol less stable when isolated than in the intact protein, whereas the isolated C-domain was ~0.45 kcal/mol more stable than in the full-length protein (*64*). They postulated that this was due to an unfolding intermediate in which interactions between the folded N-domain and the unfolded C-domain take place. Such an intermediate was indeed observed later by NMR-monitored thermal denaturation studies of *D. melanogaster* apo-calmodulin mutants (*65*, *66*). In another EF-hand protein, troponin C, an interaction between its domains that affects their stability has also been reported (*34*). Thus it appears that interdomain interactions may be an important factor in dictating the stability of some members of the EF-hand superfamily.

The C-Domain Is More Dynamic Than the N-Domain in Cdc4p. The backbone of the N-domain of Cdc4p is well ordered, with similar ^{15}N relaxation parameters whether in isolation or in its native context. The relaxation data indicate that only the loops and termini of this domain are mobile on a fast time scale. In contrast, the C-domain of Cdc4p shows a rich array of motions detected by ^{15}N relaxation analyses. First, the presence of significant conformational mobility in the millisecond to microsecond time scale in the C-domain of Cdc4p is evident by many outlying data points in an R_1R_2 plot (Figure 5), as well as by R_{ex} terms (~1.5−15 s^{-1}) in the model-free relaxation analysis for the native protein (data not shown). Interestingly, the C-domain, but not the N-domain, of vertebrate calmodulin (which shares 41% identity with Cdc4p) has also been reported to adopt two different interconverting conformations in solution, with a population ratio of 25:1 (*15*, *67*). Second, the lower than average {^{1}H}^{15}N-NOE values for residues 77−93 indicate that this region of the C-domain in Cdc4p is flexible on a nanosecond to picosecond time scale. The dynamic nature of these residues, which include those forming helix E, is confirmed by the lack of any measurable protection against HX. The motions of these residues are dampened in Cdc4p-C, as evident by higher heteronuclear NOE values, due to intramolecular binding of the residual linker. Third, and perhaps most strikingly, the amide of Gly92 has high T_1 and T_2 values, an abnormally low {^{1}H}^{15}N-NOE value, and weak signal intensity in the ^{1}H$-^{15}$N HSQC spectrum of full-length Cdc4p, indicative of significant conformational mobility. In contrast, Gly92 shows average relaxation properties in Cdc4p-C. The reduction of the mobility of this amide in the isolated Cdc4p-C is attributed to the formation of a hydrogen bond with Asp87 that accompanies a structural change to its peptide-bound conformation. However, when intramolecular binding is removed by shortening the linker in Cdc4p-Cs, the heteronuclear NOE values for residues 77−93 decrease dramatically (Figure 5A), and the amide of Gly92 is no longer detectable in the HSQC spectrum of this protein. Consistent with these relaxation studies, it is noteworthy that the C-domain has higher rms deviations than the N-domain within the NMR-derived structural ensemble of Cdc4p (0.71 ± 0.11 versus 0.41 ± 0.07 Å^2 for backbone atoms) (*23*). This was also attributed to a difference in the motional properties of the domains, leading to fewer measurable NOE and dihedral angle restraints for the C-domain.

Biological Implications of the Cdc4p Domain Structure. Cdc4p belongs to the superfamily of EF-hand proteins. Kretsinger et al. have studied extensively the evolution of these proteins (*68*−*70*), concluding that they appear to have derived from a single EF-hand motif by two cycles of gene duplication. Furthermore, these authors have classified EF-hand proteins into 45 distinct subfamilies, 13 of which are congruent with each other and are known as CTER (for containing the *c*almodulin, *t*roponin C, *e*ssential light chain, and *r*egulatory light chain subfamilies) (*68*). Cdc4p, an essential light chain of Myo2p, belongs to this CTER group. Most members of CTER have four EF-hand motifs fashioned

into globular N- and C-domains. One re-occurring theme that arises from our study of Cdc4p, as well as those on troponin C and calmodulin, is that the apo-N-domains of these proteins are generally more stable than the apo-C-domains (*34*, *64*). Furthermore, the reduced stability in the C-domain seems to be inversely related to its affinity for Ca^{2+} or for another protein (*71*). It has been shown that this difference in ligand affinity between the domains is biologically vital. For example, the C-domain of troponin C has such a high Ca^{2+} affinity that it is saturated with this metal ion even in the resting state of the muscle and, hence, constitutively bound to a portion of TnI. The more stable N-domain only binds the second amphiphilic α-helix of TnI when Ca^{2+} is present at high concentrations (*72*). Similarly, only the apo-C-domain of calmodulin binds the gating domain of the Ca^{2+}-activated K^+ membrane channel at low Ca^{2+} concentrations, and the apo-N-domain remains free. At high Ca^{2+} concentrations, the N-domain becomes Ca^{2+} loaded and binds the regulatory domain from a second molecule leading to the opening of the channel (*73*). It is also interesting to note that the N-domains of CTER proteins show more variation in their architecture than the C-domains do. For instance, in fast muscles, the essential light chain has two different isoforms that result from differential mRNA splicing. One of these isoforms has an N-terminal 45-residue extension that serves as an arm for the interaction between the essential light chain and actin (*25*). Troponin C also has additional N-terminal residues that form a fifth helix in the N-domain. This extra helix seems to increase the stability to the domain (*34*). Thus, it appears that evolution has conserved the structure and dynamics of the C-domain in CTER proteins, which has the highest ligand affinity, while changing that of the N-domain, thereby tuning the characteristics of each protein.

The domain structure of Cdc4p provides several possible avenues for its function and regulation. Desautels et al. showed that the isolated domains of Cdc4p were insufficient for *S. pombe* cytokinesis (*28*). Thus their covalent linkage is crucial. The linkage may allow cooperative, high-affinity binding of the IQ motifs in Myo2p or Myp2p by both domains of Cdc4p. The greater stability of the N-domain may also provide protection to the C-domain from proteolysis in the cell. Indeed, Desautels et al. could express the isolated N-domain in vivo, whereas the isolated C-domain could not be detected in *S. pombe* (*28*). We also failed to express the C-domain in *E. coli* without the N-terminal His_6 tag (data not shown). Alternatively, the domain structure of Cdc4p might enable it to serve as a bridge between the actin−myosin contractile ring and additional cytokinesis proteins (*29*, *30*, *49*, *74*). Indeed, Terrak et al. (*30*) observed two binding modes for the highly homologous Mlc1p, one of which had both the N- and C-domains bound to an IQ-motif peptide. In the other mode, only the C-domain was peptide bound whereas the N-domain was in an exposed position, available to interact with a potential third protein. However, such an N-domain-binding protein has not yet been identified, as yeast two-hybrid screens revealed that Cdc4p interacts with a PI 4-kinase via its C-domain and with Vps27p using both domains (*28*).

The association of Cdc4p with many partner proteins is presumably crucial in the regulation of cytokinesis. We are currently investigating the interactions of Cdc4p with its known partners to determine the role of each domain. On the basis of the properties of Cdc4p documented herein, the analogy with other EF-hand proteins, and structural studies of Mlc1p by Terrak et al. (*30*), we predict that the C-domain will be the main mediator of the interactions between this *S. pombe* ELC and its IQ-motif-containing proteins.

ACKNOWLEDGMENT

We thank Gary Yalloway and Shouming He for assistance with mass spectrometry and Wesley Errington for cloning Cdc4p into pET28a.

SUPPORTING INFORMATION AVAILABLE

$^1H-^{15}N$ HSQC spectra of Cdc4p-Cs and Cdc4p-C bound to Cu^{2+}. This material is available free of charge via the Internet at http://pubs.acs.org.

REFERENCES

1. Balasubramanian, M. K., Bi, E., and Glotzer, M. (2004) Comparative analysis of cytokinesis in budding yeast, fission yeast and animal cells, *Curr. Biol. 14*, R806−R818.
2. Wood, K. W., Cornwell, W. D., and Jackson, J. R. (2001) Past and future of the mitotic spindle as an oncology target, *Curr. Opin. Pharmacol. 1*, 370−377.
3. Guertin, D. A., Trautmann, S., and McCollum, D. (2002) Cytokinesis in eukaryotes, *Microbiol. Mol. Biol. Rev. 66*, 155−178.
4. Mulvihill, D. P., and Hyams, J. S. (2001) Shedding a little light on light chains, *Nat. Cell Biol. 3*, E10−E12.
5. Rajagopalan, S., Wachtler, V., and Balasubramanian, M. (2003) Cytokinesis in fission yeast: a story of rings, rafts and walls, *Trends Genet. 19*, 403−408.
6. Kitayama, C., Sugimoto, A., and Yamamoto, M. (1997) Type II myosin heavy chain encoded by the myo2 gene composes the contractile ring during cytokinesis in *Schizosaccharomyces pombe*, *J. Cell Biol. 137*, 1309−1319.
7. McCollum, D., Balasubramanian, M. K., Pelcher, L. E., Hemmingsen, S. M., and Gould, K. L. (1995) *Schizosaccharomyces pombe* cdc4+ gene encodes a novel EF-hand protein essential for cytokinesis, *J. Cell Biol. 130*, 651−660.
8. Naqvi, N. I., Eng, K., Gould, K. L., and Balasubramanian, M. K. (1999) Evidence for F-actin-dependent and -independent mechanisms involved in assembly and stability of the medial actomyosin ring in fission yeast, *EMBO J. 18*, 854−862.
9. Naqvi, N. I., Wong, K. C., Tang, X., and Balasubramanian, M. K. (2000) Type II myosin regulatory light chain relieves autoinhibition of myosin-heavy-chain function, *Nat. Cell Biol. 2*, 855−858.
10. Le Goff, X., Motegi, F., Salimova, E., Mabuchi, I., and Simanis, V. (2000) The *S. pombe* rlc1 gene encodes a putative myosin regulatory light chain that binds the type II myosins myo3p and myo2p, *J. Cell Sci. 113*, 4157−4163.
11. D'Souza V, M., Naqvi, N. I., Wang, H., and Balasubramanian, M. K. (2001) Interactions of Cdc4p, a myosin light chain, with IQ-domain containing proteins in *Schizosaccharomyces pombe*, *Cell Struct. Funct. 26*, 555−565.
12. Babu, Y. S., Bugg, C. E., and Cook, W. J. (1988) Structure of calmodulin refined at 2.2 Å resolution, *J. Mol. Biol. 204*, 191−204.
13. Barbato, G., Ikura, M., Kay, L. E., Pastor, R. W., and Bax, A. (1992) Backbone dynamics of calmodulin studied by N-15 relaxation using inverse detected two-dimensional NMR spectroscopy: The central helix is flexible, *Biochemistry 31*, 5269−5278.
14. Ikura, M., Kay, L. E., Krinks, M., and Bax, A. (1991) Triple-resonance multidimensional NMR study of Calmodulin complexed with the binding domain of skeletal muscle myosin light-chain kinase: Indication of a conformational change in the central helix, *Biochemistry 30*, 5498−5504.
15. Kuboniwa, H., Tjandra, N., Grzesiek, S., Ren, H., Klee, C. B., and Bax, A. (1995) Solution structure of calcium-free calmodulin, *Nat. Struct. Biol. 2*, 768−776.
16. Zhang, M., Tanaka, T., and Ikura, M. (1995) Calcium-induced conformational transition revealed by the solution structure of apo calmodulin, *Nat. Struct. Biol. 2*, 758−767.

17. Herzberg, O., and James, M. N. G. (1988) Refined crystal-structure of troponin-C from turkey skeletal-muscle at 2.0-Å resolution, *J. Mol. Biol. 203*, 761−779.
18. Satyshur, K. A., Rao, S. T., Pyzalska, D., Drendel, W., Greaser, M., and Sundaralingam, M. (1988) Refined structure of chicken skeletal-muscle troponin-C in the 2-calcium state at 2-Å resolution, *J. Biol. Chem. 263*, 1628−1647.
19. Gagne, S. M., Tsuda, S., Li, M. X., Smillie, L. B., and Sykes, B. D. (1995) Structures of the troponin-C regulatory domains in the apo and calcium-saturated states, *Nat. Struct. Biol. 2*, 784−789.
20. Slupsky, C. M., and Sykes, B. D. (1995) NMR solution structure of calcium-saturated skeletal muscle troponin C, *Biochemistry 34*, 15953−15964.
21. Rayment, I., Rypniewski, W. R., Schmidtbase, K., Smith, R., Tomchick, D. R., Benning, M. M., Winkelmann, D. A., Wesenberg, G., and Holden, H. M. (1993) 3-dimensional structure of myosin subfragment-1—a molecular motor, *Science 261*, 50−58.
22. Xie, X., Harrison, D. H., Schlichtling, I., Sweet, R. M., Kalabokis, V. N., Szentgyorgyi, A. G., and Cohen, C. (1994) Structure of the regulatory domain of scallop myosin at 2.8 Angstrom resolution, *Nature 368*, 306−312.
23. Slupsky, C. M., Desautels, M., Huebert, T., Zhao, R., Hemmingsen, S. M., and McIntosh, L. P. (2001) Structure of Cdc4p, a contractile ring protein essential for cytokinesis in *Schizosaccharomyces pombe*, *J. Biol. Chem. 276*, 5943−5951.
24. Szent-Gyorgyi, A. G. (1996) Regulation of contraction by calcium binding myosins, *Biophys. Chem. 59*, 357−363.
25. Timson, D. J. (2003) Fine-tuning the myosin motor: the role of the essential light chain in striated muscle myosin, *Biochimie 85*, 639−645.
26. Piper, R. C., Cooper, A. A., Yang, H., and Stevens, T. H. (1995) Vps27 controls vacuolar and endocytic traffic through a prevacuolar compartment in *Saccharomyces cerevisiae*, *J. Cell Biol. 131*, 603−617.
27. Swanson, K. A., Kang, R. S., Stamenova, S. D., Hicke, L., and Radhakrishnan, I. (2003) Solution structure of Vps27 UIM-ubiquitin complex important for endosomal sorting and receptor downregulation, *EMBO J. 22*, 4597−4606.
28. Desautels, M., Den Haese, J. P., Slupsky, C. M., McIntosh, L. P., and Hemmingsen, S. M. (2001) Cdc4p, a contractile ring protein essential for cytokinesis in *Schizosaccharomyces pombe*, interacts with a phosphatidylinositol 4-kinase, *J. Biol. Chem. 276*, 5932−5942.
29. Wu, J. Q., Kuhn, J. R., Kovar, D. R., and Pollard, T. D. (2003) Spatial and temporal pathway for assembly and constriction of the contractile ring in fission yeast cytokinesis, *Dev. Cell 5*, 723−734.
30. Terrak, M., Wu, G., Stafford, W. F., Lu, R. C., and Dominguez, R. (2003) Two distinct myosin light chain structures are induced by specific variations within the bound IQ motifs-functional implications, *EMBO J. 22*, 362−371.
31. Gasteiger, E., Hoogland, C., Gattiker, A., Duvaud, S., Wilkins, M. R., Appel, R. D., and Bairoch, A. (2005) *The Protein Protocols Handbook* (Walker, J. M., Ed.) Humana Press, Totowa, NJ.
32. Landon (1977) Cleavage at aspartyl-prolyl bonds, *Methods Enzymol. 47*, 145−149.
33. Santoro, M. M., and Bolen, D. W. (1992) A test of the linear extrapolation of unfolding free energy changes over an extended denaturant concentration range, *Biochemistry 31*, 4901−4907.
34. Fredricksen, R. S., and Swenson, C. A. (1996) Relationship between stability and function for isolated domains of troponin C, *Biochemistry 35*, 14012−14026.
35. Delaglio, F., Grzesiek, S., Vuister, G. W., Zhu, G., Pfeifer, J., and Bax, A. (1995) NMRPipe: a multidimensional spectral processing system based on UNIX pipes, *J. Biomol. NMR 6*, 277−293.
36. Goddard, T. D., and Kneller, D. G. (2004) SPARKY, University of California, San Francisco.
37. Farrow, N. A., Muhandiram, R., Singer, A. U., Pascal, S. M., Kay, C. M., Gish, G., Shoelson, S. E., Pawson, T., Forman-Kay, J. D., and Kay, L. E. (1994) Backbone dynamics of a free and phosphopeptide-complexed Src homology 2 domain studied by ^{15}N NMR relaxation, *Biochemistry 33*, 5984−6003.
38. Palmer, A. G. (1998) Curvefit, Columbia University, New York.
39. Dosset, P., Hus, J. C., Blackledge, M., and Marion, D. (2000) Efficient analysis of macromolecular rotational diffusion from heteronuclear relaxation data, *J. Biomol. NMR 16*, 23−28.
40. Connelly, G. P., Bai, Y., Jeng, M. F., and Englander, S. W. (1993) Isotope effects in peptide group hydrogen exchange, *Proteins 17*, 87−92.
41. Bai, Y., Milne, J. S., Mayne, L., and Englander, S. W. (1993) Primary structure effects on peptide group hydrogen exchange, *Proteins 17*, 75−86.
42. Johnson, P. E., Brun, E., MacKenzie, L. F., Withers, S. G., and McIntosh, L. P. (1999) The cellulose-binding domains from *Cellulomonas fimi* beta-1,4-glucanase CenC bind nitroxide spin-labeled cellooligosaccharides in multiple orientations, *J. Mol. Biol. 287*, 609−625.
43. Englander, S. W., and Kallenbach, N. R. (1983) Hydrogen-exchange and structural dynamics of proteins and nucleic-acids, *Q. Rev. Biophys. 16*, 521−655.
44. Daragan, V. A., and Mayo, K. H. (1997) Motional model analyses of protein and peptide dynamics using C-13 and N-15 NMR relaxation, *Prog. Nucl. Magn. Reson. Spectrosc. 31*, 63−105.
45. Kneller, J. M., Lu, M., and Bracken, C. (2002) An effective method for the discrimination of motional anisotropy and chemical exchange, *J. Am. Chem. Soc. 124*, 1852−1853.
46. Harford, C., and Sarkar, B. (1997) Amino terminal Cu(II)- and Ni(II)-binding (ATCUN) motif of proteins and peptides: Metal binding, DNA cleavage, and other properties, *Acc. Chem. Res. 30*, 123−130.
47. Donaldson, L. W., Skrynnikov, N. R., Choy, W. Y., Muhandiram, D. R., Sarkar, B., Forman-Kay, J. D., and Kay, L. E. (2001) Structural characterization of proteins with an attached ATCUN motif by paramagnetic relaxation enhancement NMR spectroscopy, *J. Am. Chem. Soc. 123*, 9843−9847.
48. Lord, M., and Pollard, T. D. (2004) UCS protein Rng3p activates actin filament gliding by fission yeast myosin-II, *J. Cell Biol. 167*, 315−325.
49. Veeraraghavan, S., Fagan, P. A., Hu, H., Lee, V., Harper, J. F., Huang, B., and Chazin, W. J. (2002) Structural independence of the two EF-hand domains of caltractin, *J. Biol. Chem. 277*, 28564−28571.
50. Lee, S. Y., and Klevit, R. E. (2000) The whole is not the simple sum of its parts in Calmodulin from *S. cerevisiae*, *Biochemistry 39*, 4225−4230.
51. Aulabaugh, A., Niemczura, W. P., and Gibbons, W. A. (1984) High field proton NMR studies of tryptic fragments of calmodulin: a comparison with the native protein, *Biochem. Biophys. Res. Commun. 118*, 225−232.
52. Finn, B. E., Evenas, J., Drakenberg, T., Waltho, J. P., Thulin, E., and Forsen, S. (1995) Calcium-induced structural-changes and domain autonomy in calmodulin, *Nat. Struct. Biol. 2*, 777−783.
53. Mal, T. K., Ikura, M., and Kay, L. E. (2002) The ATCUN domain as a probe of intermolecular interactions: application to calmodulin-peptide complexes, *J. Am. Chem. Soc. 124*, 14002−14003.
54. Tsuda, S., Hasegawa, Y., Yoshida, M., Yagi, K., and Hikichi, K. (1988) Nuclear magnetic resonance study on rabbit skeletal troponin C: calcium-induced conformational change, *Biochemistry 27*, 4120−4126.
55. Padilla, A., Cave, A., and Parello, J. (1988) Two-dimensional ^{1}H nuclear magnetic resonance study of pike pI 5.0 parvalbumin (*Esox lucius*). Sequential resonance assignments and folding of the polypeptide chain, *J. Mol. Biol. 204*, 995−1017.
56. Matei, E., Miron, S., Blouquit, Y., Duchambon, P., Durussel, I., Cox, J. A., and Craescu, C. T. (2003) C-terminal half of human centrin 2 behaves like a regulatory EF-hand domain, *Biochemistry 42*, 1439−1450.
57. Drakenberg, T., Hofmann, T., and Chazin, W. J. (1989) ^{1}H NMR studies of porcine calbindin D9k in solution: sequential resonance assignment, secondary structure, and global fold, *Biochemistry 28*, 5946−5954.
58. Strynadka, N. C., and James, M. N. (1989) Crystal structures of the helix-loop-helix calcium-binding proteins, *Annu. Rev. Biochem. 58*, 951−998.
59. Martin, S. R., Bayley, P. M., Brown, S. E., Porumb, T., Zhang, M. J., and Ikura, M. (1996) Spectroscopic characterization of a high-affinity calmodulin-target peptide hybrid molecule, *Biochemistry 35*, 3508−3517.
60. Faga, L. A., Sorensen, B. R., VanScyoc, W. S., and Shea, M. A. (2003) Basic interdomain boundary residues in calmodulin decrease calcium affinity of sites I and II by stabilizing helix-helix interactions, *Proteins 50*, 381−391.
61. Elcock, A. H. (2001) Prediction of functionally important residues based solely on the computed energetics of protein structure, *J. Mol. Biol. 312*, 885−896.

62. Li, R. H., and Woodward, C. (1999) The hydrogen exchange core and protein folding, *Protein Sci. 8*, 1571−1590.
63. Woodward, C., Carulla, N., and Barany, G. (2004) Native state hydrogen-exchange analysis of protein folding and protein motional domains, *Methods Enzymol. 380*, 379−400.
64. Masino, L., Martin, S. R., and Bayley, P. M. (2000) Ligand binding and thermodynamic stability of a multidomain protein, calmodulin, *Protein Sci. 9*, 1519−1529.
65. Fefeu, S., Biekofsky, R. R., McCormick, J. E., Martin, S. R., Bayley, P. M., and Feeney, J. (2000) Calcium-induced refolding of the calmodulin V136G mutant studied by NMR spectroscopy: evidence for interaction between the two globular domains, *Biochemistry 39*, 15920−15931.
66. Biekofsky, R. R., Martin, S. R., McCormick, J. E., Masino, L., Fefeu, S., Bayley, P. M., and Feeney, J. (2002) Thermal stability of calmodulin and mutants studied by $^{1}H-^{15}N$ HSQC NMR measurements of selectively labeled [^{15}N]Ile proteins, *Biochemistry 41*, 6850−6859.
67. Tjandra, N., Kuboniwa, H., Ren, H., and Bax, A. (1995) Rotational-dynamics of calcium-free calmodulin studied by ^{15}NNMR relaxation measurements, *Eur. J. Biochem. 230*, 1014−1024.
68. Kawasaki, H., Nakayama, S., and Kretsinger, R. H. (1998) Classification and evolution of EF-hand proteins, *Biometals 11*, 277−295.
69. Nakayama, S., Moncrief, N. D., and Kretsinger, R. H. (1992) Evolution of EF-hand calcium-modulated proteins. 2. Domains of several subfamilies have diverse evolutionary histories, *J. Mol. Evol. 34*, 416−448.
70. Moncrief, N. D., Kretsinger, R. H., and Goodman, M. (1990) Evolution of EF-hand calcium-modulated proteins. 1. Relationships based on amino-acid-sequences, *J. Mol. Evol. 30*, 522−562.
71. Vetter, S. W., and Leclerc, E. (2003) Novel aspects of calmodulin target recognition and activation, *Eur. J. Biochem. 270*, 404−414.
72. Takeda, S., Yamashita, A., Maeda, K., and Maeda, Y. (2003) Structure of the core domain of human cardiac troponin in the Ca^{2+}-saturated form, *Nature 424*, 35−41.
73. Schumacher, M. A., Rivard, A. F., Bachinger, H. P., and Adelman, J. P. (2001) Structure of the gating domain of a Ca^{2+}-activated K^{+} channel complexed with Ca^{2+}/calmodulin, *Nature 410*, 1120−1124.
74. Bhattacharya, S., Bunick, C. G., and Chazin, W. J. (2004) Target selectivity in EF-hand calcium binding proteins, *Biochim. Biophys. Acta 1742*, 69−79.
75. Wishart, D. S., Sykes, B. D., and Richards, F. M. (1992) The chemical shift index: a fast and simple method for the assignment of protein secondary structure through NMR spectroscopy, *Biochemistry 31*, 1647−1651.

BI050641C